JACS
JOURNAL OF THE AMERICAN CHEMICAL SOCIETY

Article

pubs.acs.org/JACS

Mechanism of the Iron(II)-Catalyzed Hydrosilylation of Ketones: Activation of Iron Carboxylate Precatalysts and Reaction Pathways of the Active Catalyst

Tim Bleith and Lutz H. Gade*

Anorganisch-Chemisches Institut, Universität Heidelberg, Im Neuenheimer Feld 270, 69120 Heidelberg, Germany

Supporting Information

ABSTRACT: A detailed mechanistic study of the catalytic hydrosilylation of ketones with the highly active and enantioselective iron(II) boxmi complexes as catalysts (up to >99% ee) was carried out to elucidate the pathways for precatalyst activation and the mechanism for the iron-catalyzed hydrosilylation. Carboxylate precatalysts were found to be activated by reduction of the carboxylate ligand to the corresponding alkoxide followed by entering the catalytic cycle for the iron-catalyzed hydrosilylation. An Eyring-type analysis of the temperature dependence of the enantiomeric ratio established a linear relationship of $\ln(S/R)$ and T^{-1}, indicating a single selectivity-determining step over the whole temperature range from −40 to +65 °C ($\Delta\Delta G^{\ddagger}_{\mathrm{sel,\ 233\ K}} = 9 \pm 1$ kJ/mol). The rate law as well as activation parameters for the rate-determining step were derived and complemented by a Hammett analysis, radical clock experiments, kinetic isotope effect (KIE) measurements ($k_H/k_D = 3.0 \pm 0.2$), the isolation of the catalytically active alkoxide intermediate, and DFT-modeling of the whole reaction sequence. The proposed reaction mechanism is characterized by a rate-determining σ-bond metathesis of an alkoxide complex with the silane, subsequent coordination of the ketone to the iron hydride complex, and insertion of the ketone into the Fe−H bond to regenerate the alkoxide complex.

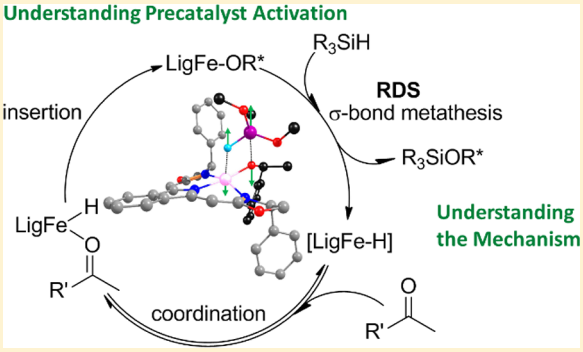

INTRODUCTION

During the course of the past decade, driven by the aim of developing catalysts based on earth abundant metals,[1,2] the use of iron complexes as catalysts has grown dramatically. Catalysts for unprecedented chemical transformations[3−5] as well as improved catalyst systems for known reactions have been reported.[6−23] However, the variety of energetically accessible oxidation and spin states of the iron center renders comprehensive mechanistic investigations difficult and our understanding of reaction mechanisms remains incomplete for most of these new applications of iron complexes.

Thorough mechanistic studies of several types of reactions have been reported, including iron-catalyzed oxidations based on the pioneering work of Que et al.[24,25] as well as, more recently, iron-catalyzed cross-coupling reactions.[26−30] However, mechanistic insight into iron-catalyzed reductions remains limited, especially for iron(II) high-spin complexes, which are promising candidates for efficient catalytic conversions due to the kinetic lability of their ligand sphere.

The development of ligand-assisted hydrogenations and transfer hydrogenations by Morris,[31,32] Milstein,[33,34] Beller,[35] Guan,[36] Schneider,[37] and Knölker/Casey[38,39] has had a major impact on iron catalysis. However, the complex species involved feature low-spin iron(II) centers with ligands, which participate in heterolytic hydrogen cleavage by providing a basic site as a proton acceptor. Especially Morris' group contributed major advances in understanding the mechanistic details of those transformations including the precatalyst activation.[40−44] Next to hydrogenations and transfer hydrogenations, hydrosilylations have been studied extensively in the context of iron catalysis, but without the same level of mechanistic understanding to date.[45−64] Besides the identification of the reaction manifold underlying the catalytic transformation and the role of the enabling ligand(s), the reactions involved in the activation of catalyst precursors provide the key to a more rational development of highly active catalysts.

Only a few mechanistic studies of iron-catalyzed hydrosilylations have been published to date, most of them focusing on iron(II) low-spin hydride complexes as catalysts. Their relatively low activity may be attributed to the robustness of the ligand sphere at the iron center leaving the first coordination sphere intact during the whole catalytic cycle.[49,65] In fact, Guan et al. showed that in their catalyst system the hydride ligand acts as a spectator ligand whereas a PMe_3 group dissociates to initiate Lewis acid catalysis,[54] although a recent computational study on this very catalyst system postulates direct involvement of the hydride, formation of an alkoxide complex, and σ-bond metathesis to yield the silyl ether.[66]

Received: February 27, 2016
Published: March 24, 2016

DOI: 10.1021/jacs.6b02173
J. Am. Chem. Soc. 2016, 138, 4972−4983

To the best of our knowledge, the only mechanistic data on iron-catalyzed hydrosilylation of ketones that were not gathered on iron(II) low-spin complexes have been reported for an iron(II) acetate/NHC catalyst system by Adolfsson et al.[67] They observed an induction period for the hydrosilylation of acetophenone while offering no explanation for this finding or further investigation of the mechanism involved.[67] Thus, at the present moment, many mechanistic features remain unclear[68] – especially for the iron(II) high-spin complexes, which have been found to be the most active catalysts for this transformation (see Scheme 1).

Scheme 1. Iron-Catalyzed Hydrosilylation of Ketones Using Fe(boxmi) Alkoxide Precatalysts

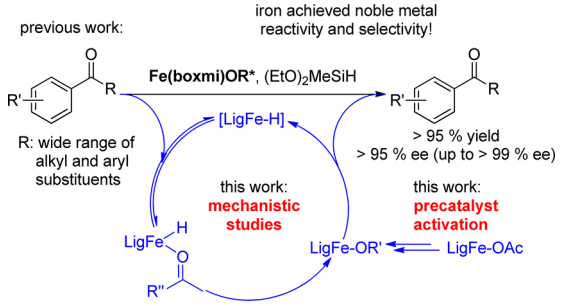

Using the boxmi ligand as a stereodirecting pincer ligand,[69−73] we recently reported the application of iron(II) boxmi complexes as catalysts in the catalytic hydrosilylation of ketones,[46] initially employing acetate complexes as precatalysts, which displayed remarkable enantioselectivity but the usual low reactivity also found for other Fe acetate precatalysts.[56,59−61,63,67] However, the corresponding alkyl or alkoxide precatalysts gave rise to highly active and enantioselective catalysts which match the top performers based on noble metals for the hydrosilylation of ketones (see Scheme 1).[46] This has led us to a systematic study of the mechanistic pathway(s) involved in the iron-catalyzed hydrosilylation of ketones as well as the activation pathway which converts the frequently employed carboxylate precatalysts to the catalytically active species.

RESULTS

The study first focuses on the reactions involved in the transformation of the iron acetate precatalysts to the corresponding active alkoxy-iron complexes because this aspect provided the key to the systematic development of highly active Fe-based systems. This is followed by a detailed mechanistic study and the proposal of a catalytic cycle for the iron-catalyzed hydrosilylation of ketones. Finally, computational modeling of the reaction pathway(s) has provided additional insight into the activity and selectivity of the boxmi-Fe catalyst.

Catalyst Activation of the Carboxylate Complexes. The reactivity of the carboxylate complexes in the hydrosilylation of ketones was monitored by ^{19}F NMR using 4′-fluoroacetophenone as the substrate (see Scheme 2). The reaction conditions were chosen to be comparable to those employed previously for iron acetate catalyzed hydrosilylations of ketones.[56,59−61,63,67]

The reaction profile shown in Figure 1 displays a characteristic induction period of approximately 5 h before the catalytic transformation started which was completed within

Scheme 2. Catalytic Hydrosilylation of 4′-Fluoroacetophenone Catalyzed by Fe(boxmi)OAc (3)

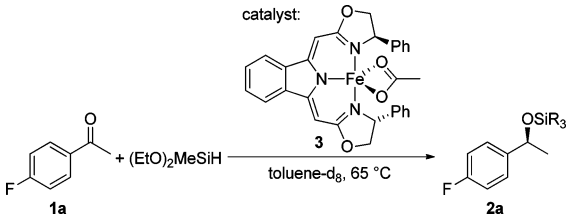

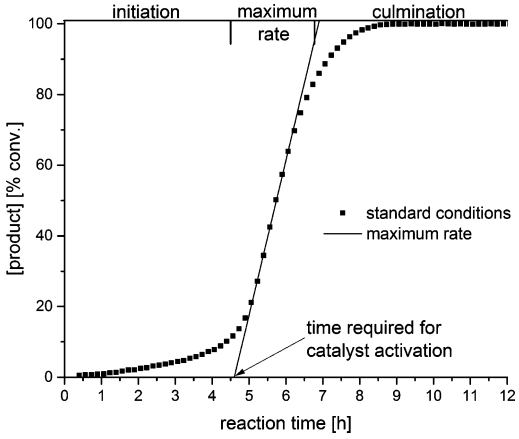

Figure 1. Reaction profile of the catalytic hydrosilylation of 4′-fluoroacetophenone (**1a**) with $(EtO)_2MeSiH$ using Fe(boxmi)OAc (**3**) as catalyst under standard conditions (65 °C, [**3**] = 6.0×10^{-3} M, [**1a**] = 0.15 M, [$(EtO)_2MeSiH$] = 0.30 M in toluene-d_8; see SI for more details). This plot also shows how the maximum rate and the time of the induction period were determined.

roughly 2 h (yielding the secondary alcohol with 90% ee). The intersection of the maximum rate tangent with the abscissa was taken as the time required for the catalyst activation.[40]

To rule out a generation of iron nanoparticles as active species in the catalytic transformation represented in Figure 1, the ee of the product was monitored throughout the transformation and was found to be independent of the conversion. Furthermore, the temperature dependence of the enantiomeric ratio was found to display "Eyring behavior" (*vide infra*) with a well-defined free activation enthalpy increment which can be associated with a single dominant catalytic pathway. This, along with the high enantioselectivity observed, is consistent with a molecularly defined catalyst system. Finally, the mercury test,[74−76] though previously argued to be of limited value for iron,[40,51,76] did not alter the outcome of the reaction.

Upon heating complex **3** and $(EtO)_2MeSiH$ for the time of the induction period and subsequent addition of the ketone (**1a**) the reaction immediately set in at a slightly higher linear maximum rate than observed without pretreatment (see Figure 1) but without the induction phase (see Figure 2). Additionally, the length of the induction period was found to depend linearly on the concentrations of the catalyst (**3**) and the silane, but to be independent of the ketone concentration (see Supporting Information (SI) for details).

We have been unable to isolate a well-defined species after treating the actetate complex **3** with $(EtO)_2MeSiH$, but the process of precatalyst activation could be monitored using ^{29}Si, ^{2}H, and ^{13}C NMR spectroscopy. To this end, the D-labeled and ^{13}C-labeled acetate complexes (**3-D$_3$** and **3-^{13}C$_1$**, respectively) were reacted with $(EtO)_2MeSiH$ at 65 °C and the reduction of

DOI: 10.1021/jacs.6b02173
J. Am. Chem. Soc. 2016, 138, 4972−4983

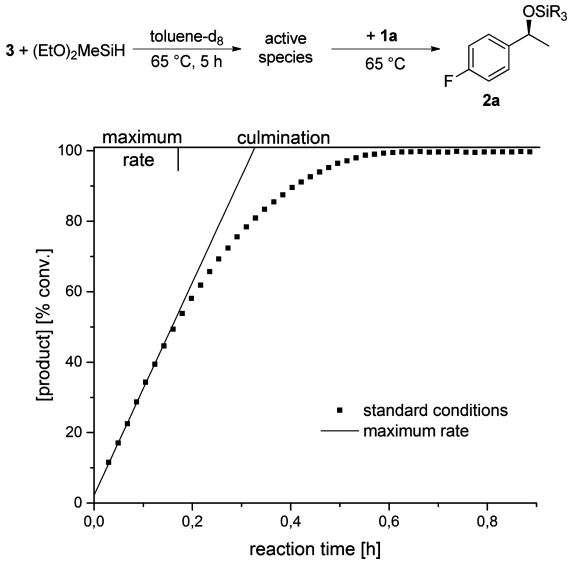

Figure 2. Reaction profile of the catalytic hydrosilylation of 4′-fluoroacetophenone (**1a**) with $(EtO)_2MeSiH$ and Fe(boxmi)OAc (**3**) as catalyst under the conditions indicated in Figure 1, but this sample was heated to 65 °C for 5 h prior to the addition of the ketone **1a**.

the acetate moiety to an ethoxy group bound to a silicon center was observed (see SI for details). Additionally, we synthesized the Fe(boxmi)OC_2D_5-complex *in situ* by reaction of Fe(boxmi)CH_2TMS (**4**) with C_2D_5OD (^2H NMR: δ (ppm) = 14.2 (CD_2), −31.8 (CD_3); see Scheme 3 and SI for more details).

Scheme 3. Reaction Sequence To Probe the Existence of an Iron Hydride Species

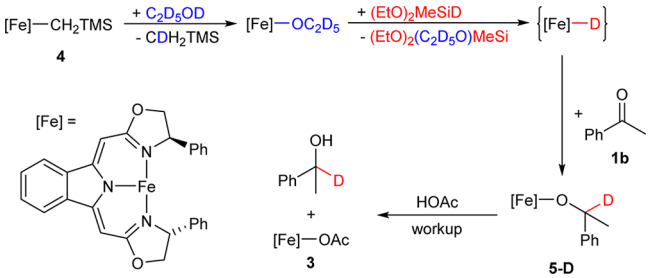

This complex was treated with a stoichiometric amount of $(EtO)_2MeSiD$ leading in a clean conversion to $(EtO)_2(C_2D_5O)MeSi$ within minutes at room temperature, which explains that signals of an iron ethoxide complex were not observed during the induction period. Unfortunately, no ^2H NMR signal or any other indicative analytics of the iron product could be obtained. Nevertheless, acetophenone (**1b**) was subsequently added and monodeuterated 1-phenylethanol was obtained after acidic cleavage of the iron alkoxide bond. This renders an iron(II) hydride species a very likely product of the conversion of the alkoxide complex with $(EtO)_2MeSiD$.

These findings led us to propose that the first step is the reduction of the acetate moiety. The concentration dependence of the induction period is first order in both **3** and $(EtO)_2MeSiH$, being consistent with a slow first reduction step of the acetate to an aldehyde or an acetal and a subsequent rapid conversion to an ethoxide. Finally, the alkoxide complex reacts with another equivalent of $(EtO)_2MeSiH$ to yield the hydride complex (see Scheme 4). We assume the conversion of the carboxylate complex to the alkoxide complex or hydride complex to be incomplete under reaction conditions; however, a quantitative determination of the conversion of the acetate complex **3** failed.

Scheme 4. Proposal for the Activation of Carboxylate Complexes in the Iron-Catalyzed Hydrosilylation

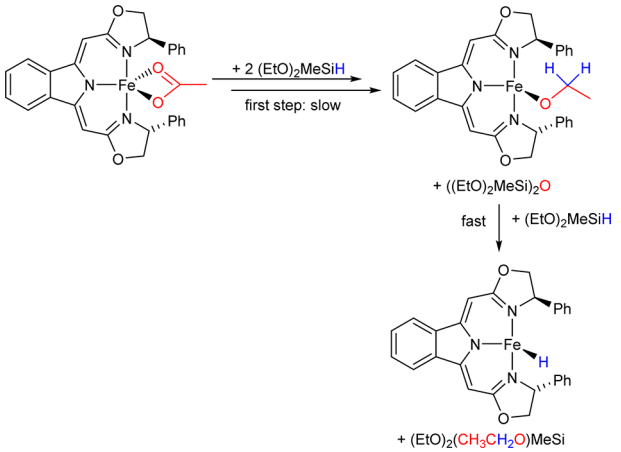

Reactivity of the Iron Alkoxide Complexes in the Hydrosilylation of Ketones. Iron boxmi alkoxide complexes are readily available via alcoholysis of the corresponding neosyl complexes **4** (neosyl-substituent = (trimethylsilyl)methyl-substituent). The molecular structure, previously determined by single crystal X-ray structure analysis of the pyridine adduct of **5**, obtained by reaction of **4** with (*S*)-1-phenylethanol, is depicted in Figure 3.[46] Complex **5** was found to catalyze the hydrosilylation of ketones at an unprecedented TOF for Fe catalysts of >240 h^{-1} at −40 °C. This gave rise to enantioselectivities for a wide range of alkyl aryl ketones of up to >99% ee.[46]

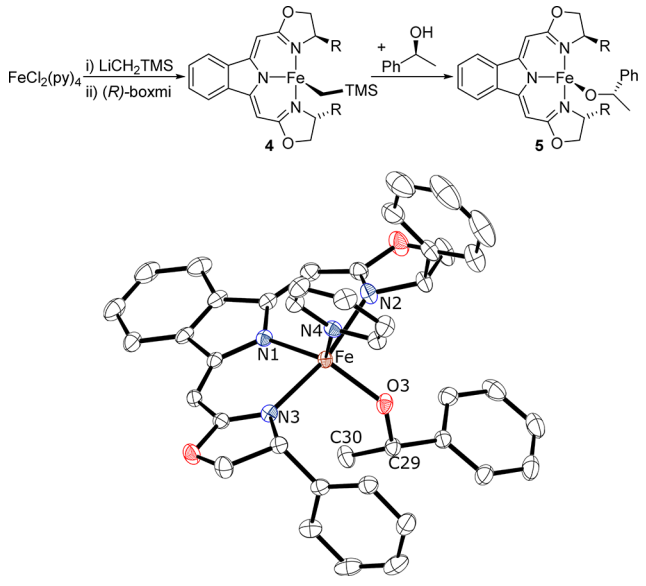

Figure 3. (Top) Synthesis of Fe(boxmi) neosyl (**4**) and alkoxide complexes (**5**). (Bottom) Molecular structure of **5(py)** at 50% probability ellipsoids; hydrogen atoms are omitted for clarity (from ref 46).

DOI: 10.1021/jacs.6b02173
J. Am. Chem. Soc. 2016, 138, 4972−4983

Reaction Kinetics: The Rate Law. Employing complex **5** for the hydrosilylation led to a drastically increased reaction rate allowing a substantial reduction of the reaction temperature.[46] However, this rendered the determination of the reaction kinetics by NMR difficult due to poor convection in an NMR tube at temperatures well below −25 °C. Consequently, no reliable and reproducible temperature profiles for the reactions could be established while significant conversion took place prior to the measurements of the first data point. Moreover, problems related to sample homogeneity were also encountered upon adding the silane to a precooled solution of the ketone and the catalyst in toluene. This led us to use *in situ* IR spectroscopy at temperatures between −45 and −25 °C tracing the CO stretching vibration of the carbonyl group. Scheme 5 summarizes the reaction conditions chosen for the kinetic measurements.

Scheme 5. Reaction Conditions for the Kinetic Measurements of the Catalytic Hydrosilylation of Acetophenone

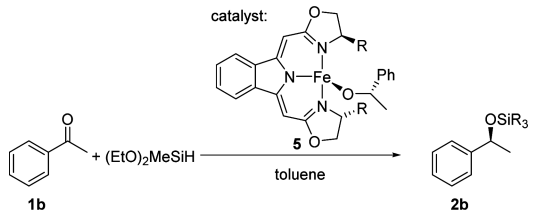

reaction conditions:		standard conditions:
[Catalyst]	1.2 x 10^{-3} - 3.9 x 10^{-3} M	2.1 x 10^{-3} M
[Ketone]	0.082 - 0.24 M	0.10 M
[$(EtO)_2$MeSiH]	0.149 - 0.298 M	0.21 M
Temperature	-45 - -25 °C	-40 °C

A reaction profile of this conversion is shown in Figure 4. When **5** was employed as a catalyst, no induction period is observed as well as rapid conversion to the silyl ether. The first five data points after the addition of the silane were used for analysis as initial rate kinetics. Since no other species than the starting material and the product were detectible by NMR, the decrease in intensity of the ν(CO) vibrational band of the ketone was taken as a probe to monitor the conversion.

Varying the concentrations of all components, we determined the rate law of the reaction by monitoring the reaction rates via low temperature *in situ* IR. First, the catalyst loading was altered in the range of 1 to 4 mol % (see Figure 5). The initial rate depends linearly on the catalyst loading, indicating first order dependence on the concentration of the catalyst.

Variation of the silane concentration also displayed a linear dependence of the initial reaction rate (see SI). However, the intersection of the linear fit was found to be displaced from the origin which we attribute to the silane consumption for the precatalyst activation.

The initial rate was found to be invariant toward a change in acetophenone concentration in the range from 0.082 to 0.24 M as shown in Figure 6 indicating zeroth order dependence of the reaction rate on the ketone concentration under the chosen conditions. This is also consistent with the linear decrease in ketone concentration during the course of the transformation as displayed in Figure 4 (bottom). It cannot be ruled out that at sufficiently low concentrations a reaction step depending on the ketone becomes rate-determining. Thus, the zeroth order

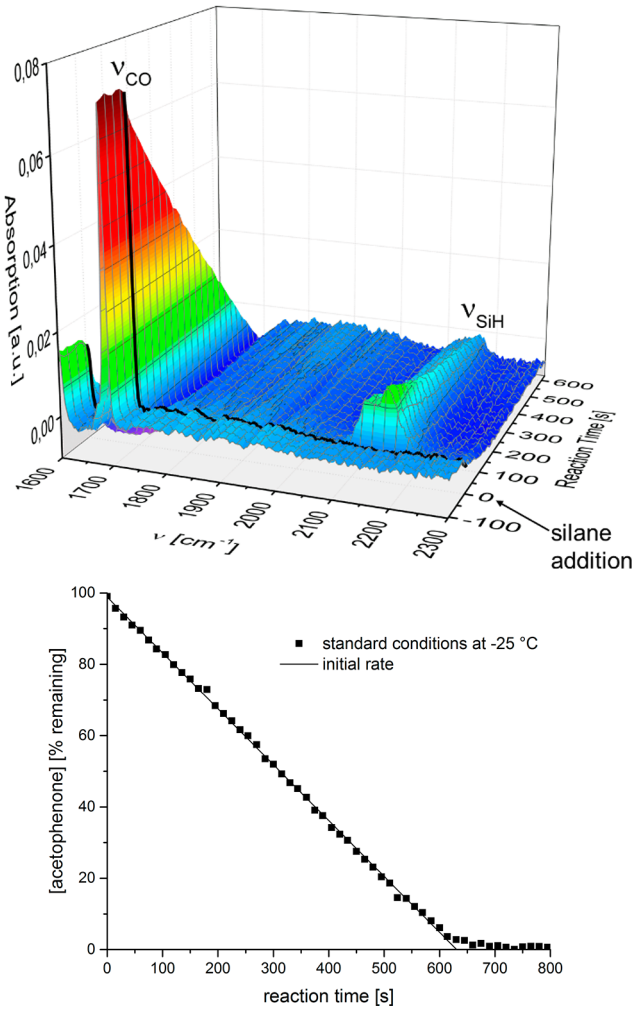

Figure 4. Reaction profile of the catalytic hydrosilylation of acetophenone (**1b**) with $(EtO)_2$MeSiH using Fe(boxmi)$OCHCH_3$Ph (**5**) as catalyst under standard conditions (Scheme 5), but at an elevated temperature of −25 °C. The time of the addition of the silane was set to zero. (Top) IR spectroscopic trace; (bottom) data integrated over the peak area of the carbonyl band.

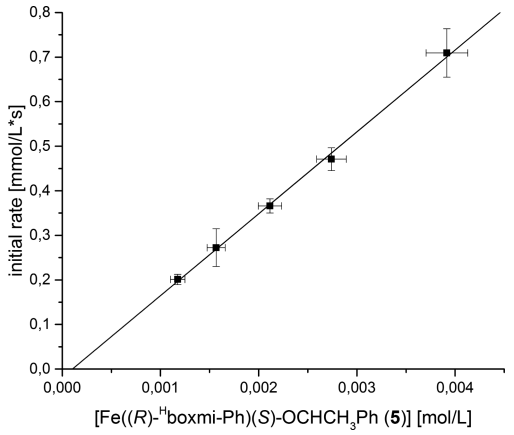

Figure 5. Initial rate depending on the catalyst loading.

dependence on the ketone concentration represents either the saturation regime of a pre-equilibrium, in which the ketone is involved, or the occurrence of two separate steps in the reaction

DOI: 10.1021/jacs.6b02173
J. Am. Chem. Soc. 2016, 138, 4972−4983

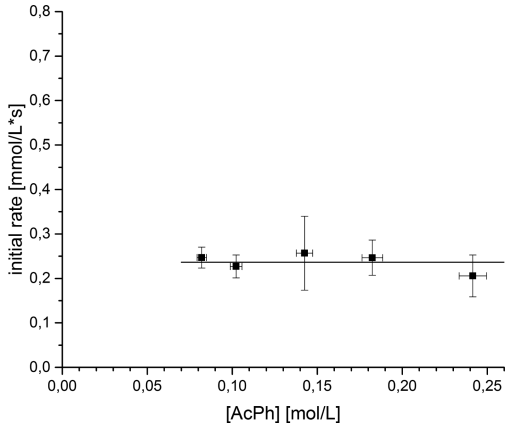

Figure 6. Initial rate as a function of acetophenone concentration.

mechanism, the one with the lower barrier involving the ketone.

From these kinetic data, the following rate law for the iron-catalyzed hydrosilylation of ketones is derived:

$$\frac{d[P]}{dt} = k\cdot[\mathrm{Fe(boxmi)OCHCH_3Ph}]\cdot[(\mathrm{EtO})_2\mathrm{MeSiH}]$$

$$k = 1.04 \pm 0.42\ \frac{\mathrm{L}}{\mathrm{mol}\cdot\mathrm{s}}$$

Activation Parameters for the Rate-Determining Step. In order to obtain further information about the rate-determining step as well as the selectivity-determining step, the reaction kinetics was studied at various temperatures and transition state parameters were determined via an Eyring plot (Figure 7), which shows a straight line indicating that there is

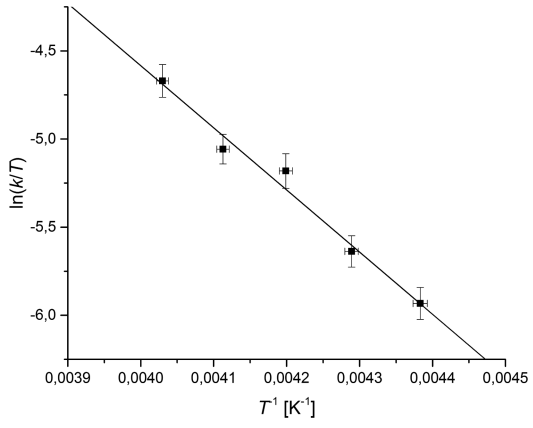

Figure 7. Eyring plot for the iron-catalyzed hydrosilylation of acetophenone in the temperature range from −45 to −25 °C.

only one rate-determining step over this temperature range. The activation parameters were found to be $\Delta H^{\ddagger} = 26 \pm 2$ kJ/mol; $\Delta S^{\ddagger} = -119 \pm 10$ J/(K·mol); $\Delta G^{\ddagger}_{233\ \mathrm{K}} = 57 \pm 3$ kJ/mol. The highly negative activation entropy indicates that the rate-determining step involves an associative process.

An Eyring-type analysis of the temperature dependence of the enantiomeric ratio,[77] depicted in Figure 8, established a linear relationship of $\ln(S/R)$ and T^{-1}, indicating a single selectivity-determining step over the whole temperature range from −40 to +65 °C, supporting the notion that the catalyst is a

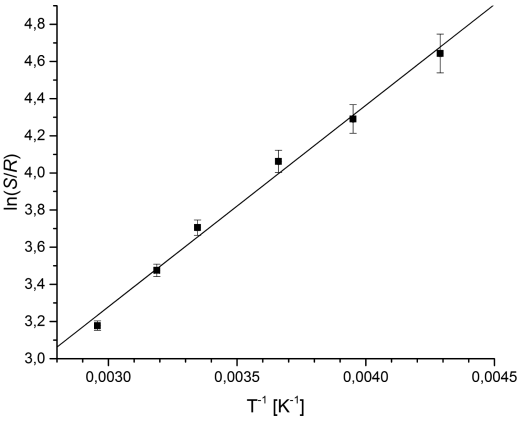

Figure 8. Eyring-type analysis of the temperature dependence of the enantiomeric ratio for the hydrosilylation of acetophenone between −40 to +65 °C under standard conditions as shown in Scheme 5.

well-defined molecular species which operates via the same mechanism over the whole temperature range.

From these data, the difference values of the activation parameters for a *re*- or *si*-face attack, respectively, were derived:[77] $\Delta\Delta H^{\ddagger}_{\mathrm{sel}} = 9 \pm 1$ kJ/mol; $\Delta\Delta S^{\ddagger}_{\mathrm{sel}} = 0 \pm 2$ J/(K·mol); $\Delta\Delta G^{\ddagger}_{\mathrm{sel,\ 233\ K}} = 9 \pm 1$ kJ/mol, in favor of the *re*-face attack over the corresponding *si*-face attack.

Hammett Correlation for the Rate-Determining Step. According to the rate law (*vide supra*), the rate-determining step is independent of the ketone concentration. Thus, the rate-determining step may not include the ketone at all, for which $\rho = 0$ would be expected, or the ketone is involved in the transition state via a pre-equilibrium or an earlier reaction step, leading to a nonzero Hammett parameter ρ. The relative reaction rates of six *para*-substituted acetophenone derivatives (MeO, Me, H, F, Cl, Br) were assessed in a competitive experiment using ^{13}C NMR spectroscopy. Hammett analysis (Figure 9) gave a linear correlation with a positive slope

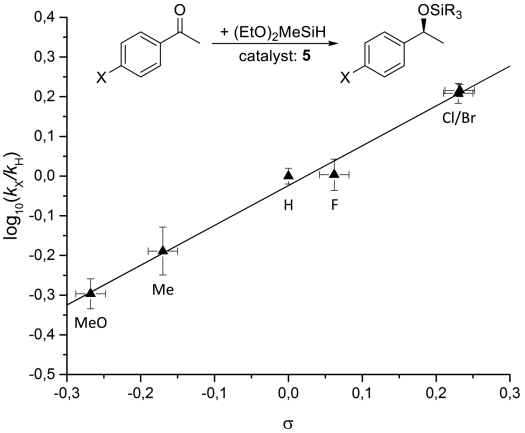

Figure 9. Hammett correlation for the iron-catalyzed hydrosilylation of various *para*-substituted acetophenone derivatives. σ-Values were taken from ref 78.

($\rho = 1.00 \pm 0.05$), which is generally interpreted in terms of a buildup of a negative charge in the rate-determining step. It also provides evidence, that the ketone is part of the active complex in the transition state of the rate-determining step.

Further Mechanistic Tests. In addition to the kinetic study described above, complementary mechanistic tests were

DOI: 10.1021/jacs.6b02173
J. Am. Chem. Soc. 2016, 138, 4972−4983

performed. Since iron is easily capable of single electron transfer (SET) reactions, a radical clock was incorporated into a ketone substrate (**6**) as a probe for radical pathways and tested under reaction conditions. Scheme 6 shows possible reaction pathways for compound **6**.

Scheme 6. Possible Reaction Pathways for the Radical Clock

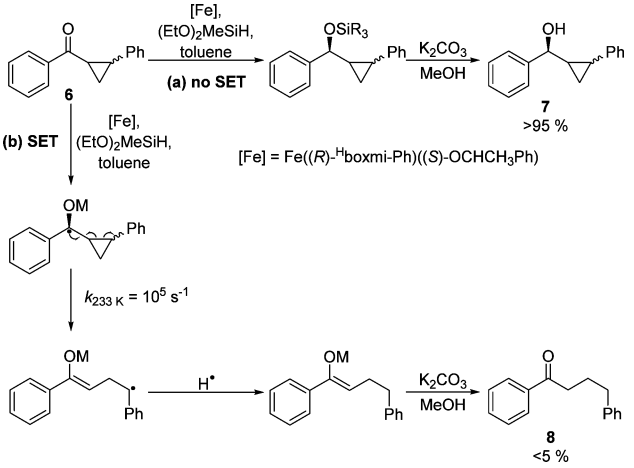

Assuming that there is no SET during the reaction, the ketone would be converted according to path (a) in Scheme 6 to the corresponding silyl ether and finally to the secondary alcohol **7**. If an SET took place, e.g. by coordination of the ketone to the iron(II) center and subsequent oxidation of Fe^{II} to Fe^{III} while reducing the ketone to the ketyl radical anion, path (b) in Scheme 6 would be followed. This pathway involves a ring opening of the cyclopropyl moiety, followed by hydrogen atom abstraction, e.g. from the solvent, to form the enolate. The latter is not subject to hydrosilylation with this catalyst and would be cleaved during workup to yield **8**. The reaction rate for the ring opening was estimated using the Arrhenius parameters given in the literature[79] to be at least 4 orders of magnitude faster than the rate-determining step of the hydrosilylation reaction. The product mixture was analyzed using HPLC and ^{2}H NMR (after quenching with K_2CO_3 in MeOD), and both confirm that less than 5% of the ring-opened product **8** were formed. The minor formation of **8** may be due to a small degree of thermal degradation of the hydride complex and the resulting generation of radical fragments. This indicates that SET is insignificant for the catalytic reaction and is consistent with the notion that the oxidation state of the iron center is not changed during its course.

The H/D kinetic isotope effect (KIE) was assessed in order to determine the contribution of a X−H bond cleavage to the transition state of the rate-determining step. Employing equal amounts $(EtO)_2MeSiH$ and $(EtO)_2MeSiD$ in the iron-catalyzed hydrosilylation established a KIE of $k_H/k_D = 3.0 \pm 0.2$, as determined by ^{13}C NMR after workup with K_2CO_3/MeOH. This implies that an X−H bond is cleaved in the rate-determining step.

As shown previously, the alkoxide complex **5** is an active intermediate. Stoichiometric treatment of **5** with $(EtO)_2MeSiH$ leads to the formation of the silyl ether of the alkoxide. Unfortunately, no well-defined iron species could be isolated from this stoichiometric reaction, and a potential high spin hydrido species thus remains elusive.[46]

Mechanistic Proposal. Taking all these pieces of information into account, we propose a mechanistic cycle for the iron-catalyzed hydrosilylation as depicted in Scheme 7

Scheme 7. Mechanistic Proposal for the Iron-Catalyzed Hydrosilylation of Ketones[a]

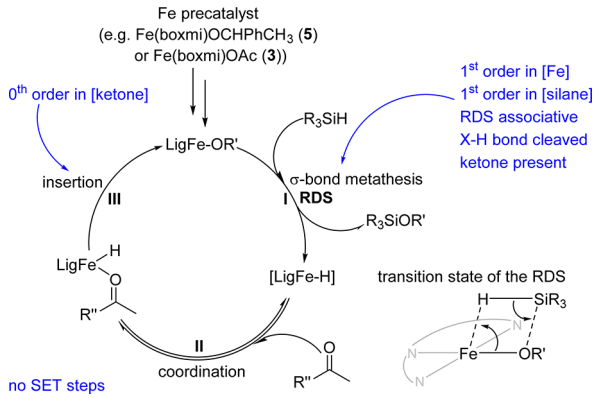

[a]Requirements for the mechanistic proposal from the experiments are shown in blue.

which consists of three steps.[46] Starting from an iron alkoxide complex the rate-determining step (RDS) takes place in which a σ-bond metathesis with a Si−H bond of a silane occurs to form the silyl ether (step **I**). This is consistent with (*i*) the reaction rate being only dependent on [Fe] and $[(EtO)_2MeSiH]$, (*ii*) the formation of an associative activated complex, (*iii*) the ketone moiety being present in the rate-determining step, (*iv*) an X−H bond being cleaved in the RDS, and finally (*v*) the formation of a silyl ether in the reaction of the alkoxide complex **5** with $(EtO)_2MeSiH$. The resulting iron hydride species, supposedly a highly reactive species, is coordinated by a ketone (step **II**), which then inserts irreversibly into the Fe−H bond to yield the alkoxide complex as resting state (step **III**). The combination of these two steps is backed by the fact that the ketone, though involved in the RDS, is incorporated in an earlier rapid step, thus not affecting the rate law. We would like to point out that Fe^{II} hydride species in the *high-spin* state are *very* rarely isolated and characterized, which attests to their high reactivity.[46,80] The cycle as proposed in Scheme 7 does not involve any single electron transfer steps, as derived from the results of the radical clock experiments.

DFT-Modeling of the Mechanistic Proposal. In order to probe the feasibility and to obtain additional insight into the proposed mechanism, the whole cycle was modeled using DFT methods. We employed a BP86[81,82]/def2-TZVP[83]//TPSSh[84,85]/def2-QZVPP/COSMO(toluene)[86,87] computational tool as implemented in ORCA 3.0.3.[88] As a minor simplification $(EtO)_2MeSiH$ was replaced by $(MeO)_2MeSiH$ in order to save computational cost due to the reduced degrees of freedom for rotations within the alkoxide substituent. The results are depicted in Figure 10, starting with the coordination of the ketone to the iron hydride complex (step **II** in Scheme 7). As expected, the coordination of an additional ligand to establish a penta-coordinated species is slightly exergonic (by 15 kJ mol^{-1}) which is consistent with the observed propensity of the four-coordinate iron complexes to bind an additional fifth ligand.

DOI: 10.1021/jacs.6b02173
J. Am. Chem. Soc. 2016, 138, 4972−4983

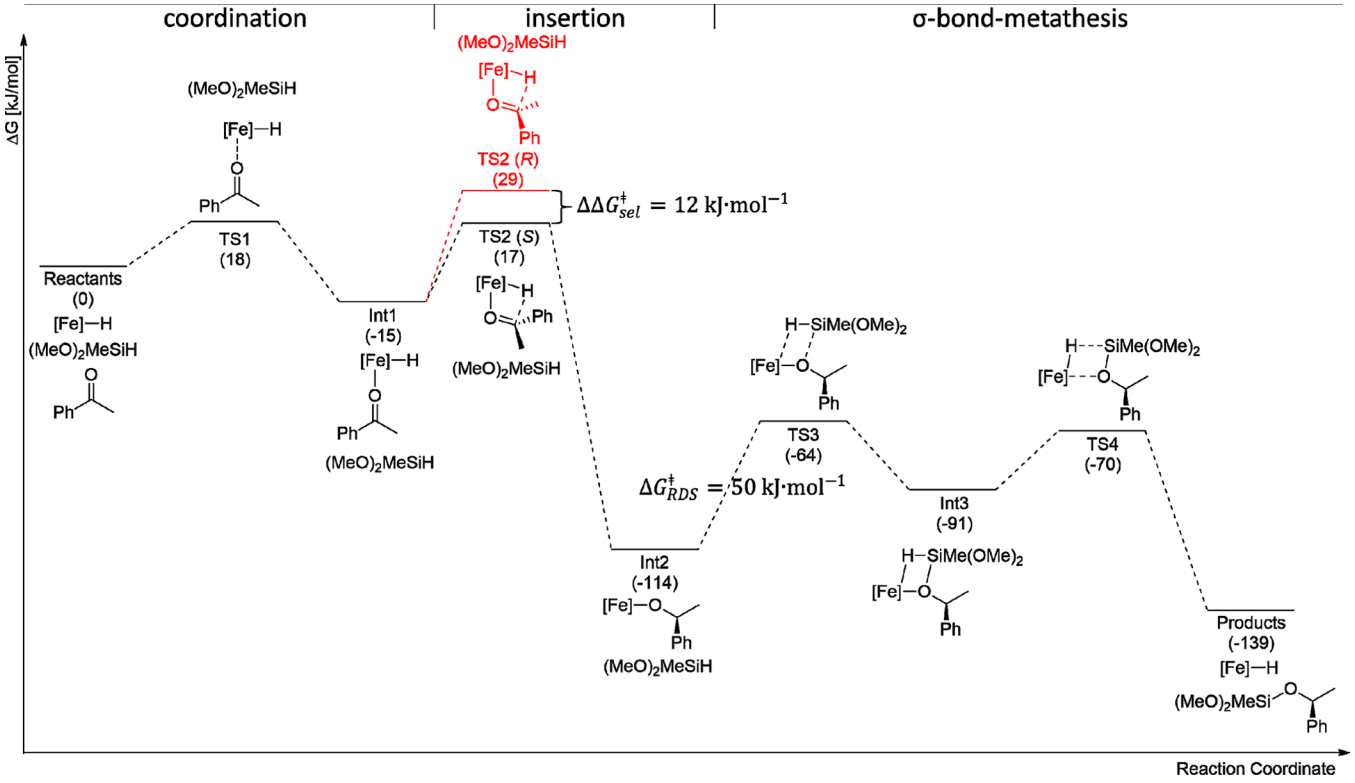

Figure 10. Gibbs free enthalpy reaction profile of the iron-catalyzed hydrosilylation of ketones. The black pathway leads to the major enantiomer, whereas the red one, leading to the minor enantiomer, is only shown for TS2. For all following steps, both pathways are very similar and, for simplicity, only the major pathway is shown (see SI for further details). All relative energy values given in brackets are given in kJ mol^{-1} (BP86/def2-TZVP//TPSSh/def2-QZVPP/COSMO(toluene)). For reasons of simplicity, this diagram starts with the coordination of the ketone (step **II** in Scheme 7).

The following insertion (step **III** in Scheme 7) of the ketone into the Fe−H bond is calculated to be irreversible with a barrier of 32 kJ mol^{-1} for the insertion and 131 kJ mol^{-1} for the reverse reaction. This is also the stereodetermining step within the catalytic cycle. From the DFT-calculations, the discrimination between the *re*- and the *si*-face attack is predicted in favor of the *re*-face attack by 12 kJ mol^{-1}. This matches the experimental value of 9 ± 1 kJ mol^{-1} within the error margin of both approaches. As to be seen from the two different transition states (see Figure 11), the stereochemical discrimination in the selectivity-determining step is mainly due to the steric repulsion between the phenyl group of the ligand and the aryl substituent of the substrate. This also explains the drop in selectivity for substrates with α-branched alkyl chains that was observed in screening the substrate scope.[46]

The theoretical model renders the σ-bond metathesis (step **I** in Scheme 7) rate-determining with a free activation enthalpy of 50 kJ mol^{-1}. Once again, the experimental value of 57 ± 3 kJ mol^{-1} is reproduced by the DFT-modeling within their error margins. After the first transition state for the coordination of the silane (see Figure 12), a shallow local minimum is present in the DFT-calculated Gibbs free enthalpy hypersurface of this system representing a four-membered cyclic intermediate of a silane adduct (Int3) which readily decomposes to yield the iron hydride complex as well as the product

The energies for all intermediates (Int2, Int3, and Int4) and transition states (TS3, TS4) for the minor stereoisomer originating from the *si*-face attack are similar to the ones of the major isomer and are therefore not displayed in Figure 10 (see SI for further details).

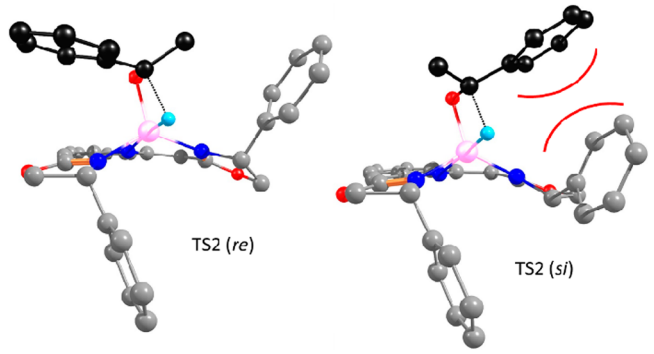

Figure 11. Structural models of the two transition states for the selectivity-determining step (step **III** in Scheme 7 or TS2 in Figure 10), showing the energetically favorable *re*-face attack on the right and the disfavored *si*-face attack on the left. Most hydrogen atoms were omitted for clarity (BP86/def2-TZVP). The carbon atoms of the boxmi ligand are displayed in gray, and the carbon atoms of the acetophenone substrate are shown in black, while nitrogen atoms are displayed in blue, oxygen atoms in red, iron in pink, and the hydride in turquoise.

DISCUSSION

Comparison of the Precatalysts. By employing alkoxide complexes (e.g., **5**) as precatalysts in the hydrosilylation of ketones, the reaction takes place at low temperatures with high selectivity. On the other hand, for carboxylate complexes (such as **3**) a long induction period is observed before a fast and selective conversion of the substrate takes place (*vide supra*). During the induction period the carboxylate complex is

DOI: 10.1021/jacs.6b02173
J. Am. Chem. Soc. 2016, 138, 4972−4983

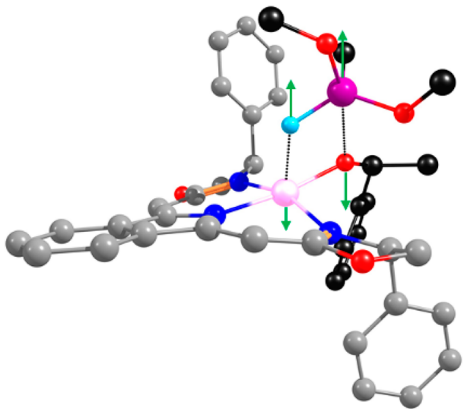

Figure 12. Structural model of the transition state for the rate-determining coordination of the silane to the iron alkoxide, initiating the σ-bond metathesis (step **I** in Scheme 7, or TS3 in Figure 10). Most hydrogen atoms were omitted for clarity (BP86/def2-TZVP). Selected displacement vectors of the imaginary frequency are shown in green. The carbon atoms of the boxmi ligand are displayed in gray, and the carbon atoms of the acetophenone substrate are shown in black, while nitrogen atoms are displayed in blue, oxygen atoms in red, iron in pink, and the hydride in turquoise.

proposed to be transformed to a hydride complex, which implies that the carboxylate complexes may also enter the mechanism for the hydrosilylation of ketones established for alkoxide complexes (see Scheme 7). In order to further corroborate this assumption, a comparison of the two precatalysts is given in Table 1.

Table 1. Comparison of the Iron Alkoxide Precatalyst (5) and the Iron Carboxylate Precatalyst (3)

	carboxylate (3)	alkoxide (5)
rate law	first order in [catalyst]	first order in [catalyst]
	first order in [silane]	first order in [silane]
	saturation in [ketone]	zeroth order in [ketone]
$\Delta S^{\ddagger}$ [J/K·mol]	112 ± 11 J/(K·mol)	119 ± 10 J/(K·mol)
Hammett ρ	1.07 ± 0.11[a]	1.00 ± 0.05[b]
radical clock	<5% opened product	<5% opened product
experiment	(8)	(8)
KIE	2.1 ± 0.2[a]	3.0 ± 0.2[b]
ee (65 °C)	92%	92%

[a]Measured at 65 °C. [b]Determined at −40 °C.

The link between carboxylate and alkoxide complexes could not be performed via stoichiometric transformation, but very similar data have been obtained for both catalyst systems (see Table 1). Kinetic studies using ^{19}F NMR spectroscopy led to a rate law with first order contributions by the catalyst concentration and the silane concentration and showing a saturation behavior for the ketone concentration (see SI for further details). An Eyring analysis of the maximum rates between 45 and 71 °C revealed a highly negative activation entropy of −112 ± 11 J/(K·mol), also confirming an associative rate-determining step.

Additionally, Hammett plots, radical clock experiments, and determination of the KIE showed very similar results to the ones found for the alkoxide complexes (see Table 1 and SI for further details). Employing Fe(boxmi)OOCEt as a precatalyst at 65 °C, a selectivity of 92% ee for 4′-phenylacetophenone was observed, which can be reproduced using **5** as a precatalyst. We therefore propose that the carboxylate complexes are first partially converted to the corresponding alkoxide complexes and then follow the hydrosilylation mechanism as proposed in Scheme 7. These findings underline the general applicability of the mechanistic proposal given in Scheme 7 for iron(II) high-spin complexes.

Discussion of Alternative Reaction Mechanisms. Four mechanisms are presented in Scheme 8 that were established previously for other catalytic hydrosilylations of ketones. In the following paragraphs, their reaction patterns are assessed relative to the findings for the iron-catalyzed hydrosilylation presented in this work. All those mechanisms do not include single electron transfer steps, ruled out by the radical clock experiment.

Scheme 8. Alternative Mechanistic Schemes Considered for the Iron-Catalyzed Hydrosilylation of Ketones

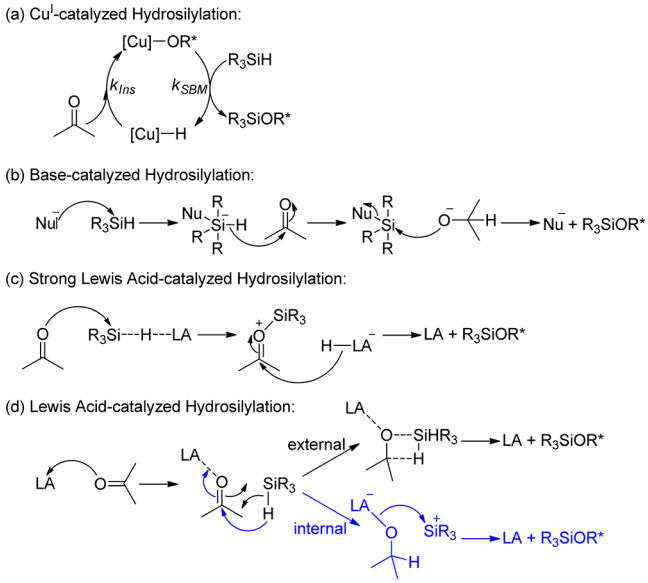

The mechanism proposed in Scheme 7 is closely related to the mechanism for Cu^{I}-catalyzed hydrosilylation [mechanism (a) in Scheme 8], as proposed and refined by Ito,[89] Lipshutz,[90] Nolan,[91] Leyssens,[92−94] and Bellemin-Laponnaz/Dedieu.[95] Notably, the KIE for the hydrosilylation catalyzed by a Cu^{I} phosphine alkoxide complex was found to be k_H/k_D = 2,[95] similar to the positive KIE observed for the iron-catalyzed reaction (*vide supra*).

Since the alkoxide as a coligand in precatalyst **5** is nucleophilic (especially toward silicon), this renders a base-catalyzed hydrosilylation pathway possible as a mechanism for this very rapid and efficient conversion [mechanism (b) in Scheme 8]. Within such a mechanistic cycle, the alkoxide coordinates to the silane to form a hypervalent hydridosilicate. This species is a much better hydride donor than the silane itself and therefore able to transfer a hydride to a ketone—even at low temperatures.[96,97] However, in order to induce a high enantioselectivity, at least one of the species involved has to be in interaction with the chiral catalyst. The most probable interaction is the coordination of the ketone to the Lewis acidic iron center. The subsequent transfer of the hydride from the hydridosilicate to the coordinated ketone is likely to be the rate-determining step. This step would display a second order dependence on the catalyst concentration, since both molecules

DOI: 10.1021/jacs.6b02173
J. Am. Chem. Soc. 2016, 138, 4972−4983

involved in this step are derived from the precatalyst: the activated ketone from the cationic iron fragment and the activated silane via the alkoxide fragment. This contradicts the findings for the rate law (see Figure 5) found in this work.

A mechanism for the hydrosilylation using very strong Lewis acids such as $B(C_6F_5)_3$,[98−102] Re^{V},[103,104] or cationic Ru^{II}[105] and Ir^{III} complexes[106,107] [mechanism (c) in Scheme 8] has been established. However, neither the rate law [proportional to $[ketone]^{-1}$] nor the requirement of a sufficiently strong Lewis acid are met in our mechanistic investigations. There are also mechanistic proposals for the ionic hydrosilylation involving an activation of the silane by oxidative addition to the metal center, which is unlikely to occur with the iron(II) high-spin complexes presented in this study.[108]

A (weak) Lewis acid catalysis at the Fe^{II} center is also a mechanistic option, which was put forward for an "external pathway"[65,109] or for an "internal pathway"[110] based on the Lewis acid activation of the ketone through coordination to make it more electrophilic [mechanism (d) in Scheme 8]. The hydride is then either transferred in a concerted pathway to yield the silyl ether directly[65] or the hydride is first transferred to form an ion pair of an anionic alcoholate Lewis acid adduct and a silylium cation, which then rearranges to the silyl ether and the Lewis acid.[110] If such a mechanism were operating, a fast and selective conversion catalyzed by the corresponding halide complexes or their derivatives obtained by addition of a halide abstraction reagent would be expected, which was not observed. Furthermore, DFT-modeling of this pathway showed that the attack of the silane on a coordinated acetophenone is energetically less favorable by more than 100 kJ mol^{-1} compared to the pathway presented in Scheme 7 and Figure 10.

CONCLUSION

Given the exceptionally high reactivity and enantioselectivity of the Fe^{II}(boxmi) alkoxide complexes in the hydrosilylation of ketones,[46] we set out to elucidate the pathways for precatalyst activation and the mechanism for the iron-catalyzed hydrosilylation involving alkoxide complexes as catalysts. We have been able to show that carboxylate complexes, such as **3**, are activated for hydrosilylation by reduction of the carboxylate ligand to the corresponding alkoxide. These complexes then enter the mechanism for the iron-catalyzed hydrosilylation as shown in Scheme 7.

In this first comprehensive kinetic study of the iron-catalyzed hydrosilylation, we derived the rate law as well as activation parameters for the rate-determining and the selectivity-determining step. Additionally, these data were complemented by a Hammett plot, application of a radical clock, KIE measurements, the isolation of a catalytic intermediate (**5**), and DFT-modeling. This has led to a well-substantiated proposal for its reaction mechanism (see Scheme 7) consisting of a rate-determining σ-bond metathesis of an alkoxide complex with the silane (step **I**), subsequent coordination of the ketone to the iron hydride complex (step **II**), and insertion of the ketone into the Fe−H bond to reestablish the alkoxide complex (step **III**).

EXPERIMENTAL SECTION

All manipulations were carried out using standard Schlenk line or drybox techniques under an atmosphere of argon. Solvents were dried over activated alumina columns using a solvent purification system (M. Braun SPS 800) or according to standard literature-known methods[111] and stored in glass ampules under an argon atmosphere. ^{1}H, $^{13}C\{^{1}H\}$, ^{19}F, ^{29}Si NMR spectra were recorded on a Bruker Avance III 600, a Bruker Avance II 400, or a Bruker DRX 200 spectrometer. ^{1}H and ^{13}C NMR spectra were referenced internally to residual protio-solvent (^{1}H) or solvent (^{13}C) resonances and are reported relative to tetramethylsilane. ^{19}F NMR resonances are reported relative to external CCl_3F (0 ppm), and ^{29}Si NMR resonances to tetramethylsilane (0 ppm). HPLC analyses were conducted on an Agilent 1200 Series chromatograph using chiral Daicel (AD-H, OD-H, OJ-H) according to the methods previously reported[46] or an achiral Macherey-Nagel column (Nucleodur 100-5). **3**,[72] **4**,[46] **5**,[46] **6**,[112] and **7**[113] were synthesized according to the literature procedures. All other reagents were commercially available and used as received. Liquids were degassed by three freeze−pump−thaw cycles prior to use. All iron salts were purchased with a trace metal purity of 99.99% or higher.

General procedure for the preparation of acetate labeled derivatives of **3**: Fe(boxmi)Cl (0.3 mmol) and NaOAc−$^{13}C_1$ or NaOAc-D_3 (0.4 mmol) were dissolved in 7 mL of abs. MeOH and stirred for 20 min at room temperature. The dark solution was evaporated to dryness, and the residue was extracted with toluene three times and filtered over Celite. After evaporation and drying *in vacuo*, a black powder was obtained.

Preparation of $(EtO)_2MeSiD$: $(EtO)_2MeSiH$ (2.5 mL, 15.6 mmol, degassed) and $Rh(PPh_3)_3Cl$ (1.01 g, 1.1 mmol) were suspended in tetraglyme (15 mL, dried over Na, degassed). Under vigorous stirring, the mixture was pressurized with 15 bar of D_2 for 7 days, with replacement of the atmosphere every 2 days. The product was separated using a bulb-to-bulb distillation. A 1.1 g amount (8.1 mmol, 52% yield) of a colorless liquid was obtained. The degree of deuteration was determined using ^{1}H NMR spectroscopy and was found to be higher than 98%.

^{1}H NMR (600.13 MHz, $CDCl_3$, 295 K): δ (ppm) 3.82−3.77 (m, 4H, OCH_2), 1.22 (t, $^{3}J_{HH}$ = 7.0 Hz, 6H, OCH_2CH_3), 0.19 (s, 3H, $SiCH_3$). ^{2}H NMR (92.12 MHz, $CHCl_3$, 295 K): δ (ppm) 4.62. ^{13}C NMR (150.92 MHz, $CDCl_3$, 295 K): δ (ppm) 59.24 (OCH_2), 18.37 (OCH_2CH_3), −3.15 (t, $^{2}J_{DC}$ = 2.6 Hz, $SiCH_3$). ^{29}Si NMR (79.44 MHz, $CDCl_3$, 295 K): δ (ppm) −16.18 (t, $^{1}J_{DSi}$ = 36.0 Hz). HRMS (EI^+): 135.0850 (1.7%, calcd for $[M]^+$: 135.0826), 133.0676 (100%, calcd. for $[M - D]^+$: 133.0685), 120.0576 (83.3%, calcd for $[M - CH_3]^+$: 120.0591), 90.0469 (33.4%, calcd for $[M - OEt]^+$: 90.0485).

General procedure for the kinetic measurements using **5** as the catalyst: A flame-dried reaction flask was equipped with a magnetic stir bar and an IR-probe of an iC-IR-spectrometer (Mettler Toledo ReactIRTM 15 with a SiCompTM probe head, connected via DST-AgX-fiber optics (9.5 mm diameter)), purged five times with vacuum/argon and cooled to the desired temperature (usually −40 °C) using a cryostat. A 3 mL aliquot of abs. toluene was added, and after thermal equilibration of at least 5 min, a background with 512 scans was collected between 1800 and 1600 cm^{-1} at 4 cm^{-1} intervals. Subsequently the iron catalyst was added as a solution in 1 mL of abs. toluene and the desired amount of acetophenone. From this point, 30 scans were collected every 15 s. After at least 5 min, $(EtO)_2MeSiH$ was added, resulting in the decrease of the peak at 1692 cm^{-1}. The peak area was used to assess the acetophenone concentration.

Procedure for the Hammett studies: **5** (7.8 mg, 13 μmol), 1,3,5-tri(methoxy)benzene (14.0 mg, 83 μmol) as the internal standard, and the ketones (20−35 mg each, 140−180 μmol each) were dissolved in 0.7 mL of toluene-d_8 in a J. Young NMR tube. A reference spectrum was measured. The solution was transferred to a vial, cooled to −40 °C, and $(EtO)_2MeSiH$ (10 μL, 62 μmol) was added at low temperature. A ^{13}C NMR spectrum of this solution was recorded. The procedure to add silane was repeated three times, and all three data points were taken into account for the analysis. The values given in the paper are an average of three independent runs.

Procedure for KIE experiments: **5** (2.6 mg, 4.3 μmol) and 4′-phenyl-acetophenone (25.0 mg, 127 μmol) were dissolved in 1.0 mL of toluene and cooled to −78 °C. A mixture of 40 μL of $(EtO)_2MeSiH$ (250 μmol), 40 μL of $(EtO)_2MeSiD$ (250 μmol), and 100 μL of toluene was added dropwise. The mixture was allowed to warm to room temperature in the cold bath within 5 h. After the mixture was stirred for 1 h at room temperature, 0.5 mL of a saturated K_2CO_3 solution in MeOH was added. Filtration through a plug of silica and

DOI: 10.1021/jacs.6b02173
J. Am. Chem. Soc. 2016, 138, 4972−4983

subsequent column chromatography yielded the desired product. The ratio of deuterated to normal product was determined by ^{13}C NMR spectroscopy and averaged over two independent runs.

Computational Details. We employed a BP86[81,82]/def2-TZVP[83]//TPSSh[84,85]/def2-QZVPP/COSMO (toluene, ε = 2.4, refractive index = 1.497)[86,87] computational tool as implemented in ORCA 3.0.3.[88] The RI[114] and the RIJCOSX approximation[115] were used as implemented in ORCA 3.0.3. One minor simplification was used for the modeling: $(EtO)_2MeSiH$ was replaced by $(MeO)_2MeSiH$ in order to save computational cost due to the reduced degrees of freedom for rotations within the alkoxide substituent. All stationary points were confirmed by frequency calculations showing no negative frequencies; transition states were found to have one negative frequency. Visualization was done using Chemcraft.[116]

Further information on the experimental and computational procedures as well as the coordinates of the optimized geometries for all intermediates and transition states can be found in the SI.

■ ASSOCIATED CONTENT

Supporting Information

The Supporting Information is available free of charge on the ACS Publications website at DOI: 10.1021/jacs.6b02173.

Cartesian coordinates of the stationary points and transition states of the computational modeling in Figure 10 (XYZ)

Methods, relevant spectra, additional information, optimized geometries from the modeling (PDF)

■ AUTHOR INFORMATION

Corresponding Author

*lutz.gade@uni-heidelberg.de

Notes

The authors declare no competing financial interest.

■ ACKNOWLEDGMENTS

We acknowledge funding by the Deutsche Forschungsgemeinschaft (Grant DFG Ga 488/9-1). T.B. thanks the Fonds der Chemischen Industrie for the doctoral Kekulé fellowship and the Studienstiftung des Deutschen Volkes for a doctoral fellowship. The computational studies were supported by the bwHPC initiative and the bwHPC-C5 project provided through the associated compute services of the JUSTUS HPC facility at the University of Ulm. bwHPC and bwHPC-C5 (http://www.bwhpc-c5.de) are funded by the Ministry of Science, Research and the Arts Baden-Württemberg (MWK) and the German Research Foundation (DFG). The authors thank Dr. Matthias Kruck for initial testing of iron-catalyzed hydrosilylation and Philip Hindenberg and Niko Jonasson for assistance with setting up the kinetic measurement systems as well as the kinetic measurements themselves.

■ REFERENCES

(1) Bullock, R. M. *Catalysis without precious metals*; Wiley-VCH: Weinheim, 2010.

(2) Bullock, R. M. *Science* **2013**, *342* (6162), 1054−1055.

(3) Yu, R. P.; Hesk, D.; Rivera, N.; Pelczer, I.; Chirik, P. J. *Nature* **2016**, *529* (7585), 195−199.

(4) Hoyt, J. M.; Schmidt, V. A.; Tondreau, A. M.; Chirik, P. J. *Science* **2015**, *349* (6251), 960−963.

(5) Hoyt, J. M.; Sylvester, K. T.; Semproni, S. P.; Chirik, P. J. *J. Am. Chem. Soc.* **2013**, *135* (12), 4862−4877.

(6) Bauer, I.; Knölker, H.-J. *Chem. Rev.* **2015**, *115* (9), 3170−3387.

(7) Greenhalgh, M. D.; Jones, A. S.; Thomas, S. P. *ChemCatChem* **2015**, *7* (2), 190−222.

(8) Chakraborty, S.; Bhattacharya, P.; Dai, H.; Guan, H. *Acc. Chem. Res.* **2015**, *48* (7), 1995−2003.

(9) Chirik, P. J. *Acc. Chem. Res.* **2015**, *48* (6), 1687−1695.

(10) Riener, K.; Haslinger, S.; Raba, A.; Högerl, M. P.; Cokoja, M.; Herrmann, W. A.; Kühn, F. E. *Chem. Rev.* **2014**, *114* (10), 5215−5272.

(11) Gopalaiah, K. *Chem. Rev.* **2013**, *113* (5), 3248−3296.

(12) Nishiyama, H. In *Comprehensive Chirality*; Carreira, E. M., Yamamoto, H., Eds.; Elsevier: Amsterdam, 2012; pp 318−333.

(13) Darwish, M.; Wills, M. *Catal. Sci. Technol.* **2012**, *2* (2), 243−255.

(14) Le Bailly, B. A. F.; Thomas, S. P. *RSC Adv.* **2011**, *1* (8), 1435−1445.

(15) Junge, K.; Schröder, K.; Beller, M. *Chem. Commun.* **2011**, *47* (17), 4849−4859.

(16) Chirik, P. J.; Wieghardt, K. *Science* **2010**, *327* (5967), 794−795.

(17) Morris, R. H. *Chem. Soc. Rev.* **2009**, *38* (8), 2282−2291.

(18) Bolm, C. *Nat. Chem.* **2009**, *1* (5), 420−420.

(19) *Iron catalysis in organic chemistry*; Plietker, B., Ed.; WILEY-VCH: Weinheim, 2008.

(20) Enthaler, S.; Junge, K.; Beller, M. *Angew. Chem., Int. Ed.* **2008**, *47* (18), 3317−3321.

(21) Bolm, C.; Legros, J.; Le Paih, J.; Zani, L. *Chem. Rev.* **2004**, *104* (12), 6217−6254.

(22) Tondreau, A. M.; Atienza, C. C. H.; Weller, K. J.; Nye, S. A.; Lewis, K. M.; Delis, J. G. P.; Chirik, P. J. *Science* **2012**, *335* (6068), 567−570.

(23) Liu, T.; DuBois, D. L.; Bullock, R. M. *Nat. Chem.* **2013**, *5* (3), 228−233.

(24) Costas, M.; Mehn, M. P.; Jensen, M. P.; Que, L. *Chem. Rev.* **2004**, *104* (2), 939−986.

(25) McDonald, A. R.; Que, L., Jr. *Coord. Chem. Rev.* **2013**, *257* (2), 414−428.

(26) Cassani, C.; Bergonzini, G.; Wallentin, C.-J. *ACS Catal.* **2016**, *6*, 1640−1648.

(27) Kneebone, J. L.; Fleischauer, V. E.; Daifuku, S. L.; Shaps, A. A.; Bailey, J. M.; Iannuzzi, T. E.; Neidig, M. L. *Inorg. Chem.* **2016**, *55* (1), 272−282.

(28) Daifuku, S. L.; Kneebone, J. L.; Snyder, B. E. R.; Neidig, M. L. *J. Am. Chem. Soc.* **2015**, *137* (35), 11432−11444.

(29) Adams, C. J.; Bedford, R. B.; Carter, E.; Gower, N. J.; Haddow, M. F.; Harvey, J. N.; Huwe, M.; Cartes, M. Á.; Mansell, S. M.; Mendoza, C.; Murphy, D. M.; Neeve, E. C.; Nunn, J. *J. Am. Chem. Soc.* **2012**, *134* (25), 10333−10336.

(30) Kleimark, J.; Hedström, A.; Larsson, P.-F.; Johansson, C.; Norrby, P.-O. *ChemCatChem* **2009**, *1* (1), 152−161.

(31) Zuo, W.; Lough, A. J.; Li, Y. F.; Morris, R. H. *Science* **2013**, *342* (6162), 1080−1083.

(32) Morris, R. H. *Acc. Chem. Res.* **2015**, *48* (5), 1494−1502.

(33) Zell, T.; Ben-David, Y.; Milstein, D. *Angew. Chem., Int. Ed.* **2014**, *53* (18), 4685−4689.

(34) Zell, T.; Milstein, D. *Acc. Chem. Res.* **2015**, *48* (7), 1979−1994.

(35) Werkmeister, S.; Junge, K.; Wendt, B.; Alberico, E.; Jiao, H.; Baumann, W.; Junge, H.; Gallou, F.; Beller, M. *Angew. Chem., Int. Ed.* **2014**, *53* (33), 8722−8726.

(36) Chakraborty, S.; Dai, H.; Bhattacharya, P.; Fairweather, N. T.; Gibson, M. S.; Krause, J. A.; Guan, H. *J. Am. Chem. Soc.* **2014**, *136* (22), 7869−7872.

(37) Chakraborty, S.; Lagaditis, P. O.; Förster, M.; Bielinski, E. A.; Hazari, N.; Holthausen, M. C.; Jones, W. D.; Schneider, S. *ACS Catal.* **2014**, *4* (11), 3994−4003.

(38) Casey, C. P.; Guan, H. *J. Am. Chem. Soc.* **2007**, *129* (18), 5816−5817.

(39) Knölker, H.-J.; Heber, J.; Mahler, C. H. *Synlett* **1992**, *1992* (12), 1002−1004.

(40) Mikhailine, A. A.; Maishan, M. I.; Lough, A. J.; Morris, R. H. *J. Am. Chem. Soc.* **2012**, *134* (29), 12266−12280.

(41) Prokopchuk, D. E.; Morris, R. H. *Organometallics* **2012**, *31*, 7375.

DOI: 10.1021/jacs.6b02173
J. Am. Chem. Soc. 2016, 138, 4972−4983

(42) Sonnenberg, J. F.; Coombs, N.; Dube, P. A.; Morris, R. H. *J. Am. Chem. Soc.* **2012**, *134* (13), 5893−5899.
(43) Lagaditis, P. O.; Sues, P. E.; Sonnenberg, J. F.; Wan, K. Y.; Lough, A. J.; Morris, R. H. *J. Am. Chem. Soc.* **2014**, *136* (4), 1367−1380.
(44) Zuo, W.; Prokopchuk, D. E.; Lough, A. J.; Morris, R. H. *ACS Catal.* **2016**, *6* (1), 301−314.
(45) Ito, J.; Hosokawa, S.; Khalid, H. B.; Nishiyama, H. *Organometallics* **2015**, *34* (7), 1377−1383.
(46) Bleith, T.; Wadepohl, H.; Gade, L. H. *J. Am. Chem. Soc.* **2015**, *137* (7), 2456−2459.
(47) Zuo, Z.; Zhang, L.; Leng, X.; Huang, Z. *Chem. Commun.* **2015**, *51* (24), 5073−5076.
(48) Zhao, H.; Sun, H.; Li, X. *Organometallics* **2014**, *33* (13), 3535−3539.
(49) Gallego, D.; Inoue, S.; Blom, B.; Driess, M. *Organometallics* **2014**, *33* (23), 6885−6897.
(50) César, V.; Misal Castro, L. C.; Dombray, T.; Sortais, J.-B.; Darcel, C.; Labat, S.; Miqueu, K.; Sotiropoulos, J.-M.; Brousses, R.; Lugan, N.; Lavigne, G. *Organometallics* **2013**, *32* (16), 4643−4655.
(51) Ruddy, A. J.; Kelly, C. M.; Crawford, S. M.; Wheaton, C. A.; Sydora, O. L.; Small, B. L.; Stradiotto, M.; Turculet, L. *Organometallics* **2013**, *32* (19), 5581−5588.
(52) Blom, B.; Enthaler, S.; Inoue, S.; Irran, E.; Driess, M. *J. Am. Chem. Soc.* **2013**, *135* (17), 6703−6713.
(53) Jiang, F.; Bézier, D.; Sortais, J.-B.; Darcel, C. *Adv. Synth. Catal.* **2011**, *353* (2−3), 239−244.
(54) Bhattacharya, P.; Krause, J. A.; Guan, H. *Organometallics* **2011**, *30* (17), 4720−4729.
(55) Dieskau, A. P.; Begouin, J.-M.; Plietker, B. *Eur. J. Org. Chem.* **2011**, *2011* (27), 5291−5296.
(56) Hosokawa, S.; Ito, J.; Nishiyama, H. *Organometallics* **2010**, *29* (22), 5773−5775.
(57) Yang, J.; Tilley, T. D. *Angew. Chem., Int. Ed.* **2010**, *49* (52), 10186−10188.
(58) Tondreau, A. M.; Darmon, J. M.; Wile, B. M.; Floyd, S. K.; Lobkovsky, E.; Chirik, P. J. *Organometallics* **2009**, *28* (13), 3928−3940.
(59) Langlotz, B. K.; Wadepohl, H.; Gade, L. H. *Angew. Chem., Int. Ed.* **2008**, *47* (25), 4670−4674.
(60) Shaikh, N. S.; Enthaler, S.; Junge, K.; Beller, M. *Angew. Chem., Int. Ed.* **2008**, *47* (13), 2497−2501.
(61) Furuta, A.; Nishiyama, H. *Tetrahedron Lett.* **2008**, *49* (1), 110−113.
(62) Tondreau, A. M.; Lobkovsky, E.; Chirik, P. J. *Org. Lett.* **2008**, *10* (13), 2789−2792.
(63) Nishiyama, H.; Furuta, A. *Chem. Commun.* **2007**, *7*, 760−762.
(64) Brunner, H.; Fisch, K. *J. Organomet. Chem.* **1991**, *412* (1−2), C11−C13.
(65) Metsänen, T. T.; Gallego, D.; Szilvási, T.; Driess, M.; Oestreich, M. *Chem. Sci.* **2015**, *6* (12), 7143−7149.
(66) Wang, W.; Gu, P.; Wang, Y.; Wei, H. *Organometallics* **2014**, *33* (4), 847−857.
(67) Buitrago, E.; Tinnis, F.; Adolfsson, H. *Adv. Synth. Catal.* **2012**, *354* (1), 217−222.
(68) Chakraborty, S.; Guan, H. *Dalton Trans.* **2010**, *39* (32), 7427.
(69) Deng, Q.-H.; Melen, R. L.; Gade, L. H. *Acc. Chem. Res.* **2014**, *47*, 3162−3173.
(70) Deng, Q.-H.; Wadepohl, H.; Gade, L. H. *J. Am. Chem. Soc.* **2012**, *134*, 2946−2949.
(71) Deng, Q.-H.; Wadepohl, H.; Gade, L. H. *J. Am. Chem. Soc.* **2012**, *134*, 10769−10772.
(72) Deng, Q.-H.; Bleith, T.; Wadepohl, H.; Gade, L. H. *J. Am. Chem. Soc.* **2013**, *135*, 5356−5359.
(73) Deng, Q.-H.; Rettenmeier, C.; Wadepohl, H.; Gade, L. H. *Chem. - Eur. J.* **2014**, *20*, 93−97.
(74) Foley, P.; DiCosimo, R.; Whitesides, G. M. *J. Am. Chem. Soc.* **1980**, *102* (22), 6713−6725.
(75) Anton, D. R.; Crabtree, R. H. *Organometallics* **1983**, *2* (7), 855−859.
(76) Widegren, J. A.; Finke, R. G. *J. Mol. Catal. A: Chem.* **2003**, *198* (1−2), 317−341.
(77) Göbel, T.; Sharpless, K. B. *Angew. Chem., Int. Ed. Engl.* **1993**, *32* (9), 1329−1331.
(78) Hansch, C.; Leo, A.; Taft, R. W. *Chem. Rev.* **1991**, *91*, 165−195.
(79) Tanner, D. D.; Chen, J. J.; Luelo, C.; Peters, P. M. *J. Am. Chem. Soc.* **1992**, *114* (2), 713−717.
(80) Smith, J. M.; Lachicotte, R. J.; Holland, P. L. *J. Am. Chem. Soc.* **2003**, *125* (51), 15752−15753.
(81) Becke, A. D. *Phys. Rev. A: At., Mol., Opt. Phys.* **1988**, *38*, 3098−3100.
(82) Perdew, J. P. *Phys. Rev. B: Condens. Matter Mater. Phys.* **1986**, *33*, 8822−8824.
(83) Weigend, F.; Ahlrichs, R. *Phys. Chem. Chem. Phys.* **2005**, *7*, 3297−3305.
(84) Staroverov, V. N.; Scuseria, G. E.; Tao, J.; Perdew, J. P. *J. Chem. Phys.* **2003**, *119*, 12129−12137.
(85) Staroverov, V. N.; Scuseria, G. E.; Tao, J.; Perdew, J. P. *J. Chem. Phys.* **2004**, *121*, 11507−11507.
(86) Klamt, A.; Schüürmann, G. *J. Chem. Soc., Perkin Trans. 2* **1993**, 799−805.
(87) Sinnecker, S.; Rajendran, A.; Klamt, A.; Diedenhofen, M.; Neese, F. *J. Phys. Chem. A* **2006**, *110*, 2235−2245.
(88) Neese, F. *Wiley Interdiscip. Rev. Comput. Mol. Sci.* **2012**, *2*, 73−78.
(89) Ito, H.; Ishizuka, T.; Okumura, T.; Yamanaka, H.; Tateiwa, J.; Sonoda, M.; Hosomi, A. *J. Organomet. Chem.* **1999**, *574* (1), 102−106.
(90) Lipshutz, B. H.; Noson, K.; Chrisman, W.; Lower, A. *J. Am. Chem. Soc.* **2003**, *125* (29), 8779−8789.
(91) Díez-González, S.; Nolan, S. P. *Acc. Chem. Res.* **2008**, *41* (2), 349−358.
(92) Vergote, T.; Gathy, T.; Nahra, F.; Riant, O.; Peeters, D.; Leyssens, T. *Theor. Chem. Acc.* **2012**, *131* (7), 1−13.
(93) Vergote, T.; Gharbi, S.; Billard, F.; Riant, O.; Leyssens, T. *J. Organomet. Chem.* **2013**, *745−746*, 133−139.
(94) Vergote, T.; Nahra, F.; Merschaert, A.; Riant, O.; Peeters, D.; Leyssens, T. *Organometallics* **2014**, *33*, 1953.
(95) Issenhuth, J.-T.; Notter, F.-P.; Dagorne, S.; Dedieu, A.; Bellemin-Laponnaz, S. *Eur. J. Inorg. Chem.* **2010**, *2010* (4), 529−541.
(96) Revunova, K.; Nikonov, G. I. *Chem. - Eur. J.* **2014**, *20* (3), 839−845.
(97) Chuit, C.; Corriu, R. J. P.; Reye, C.; Young, J. C. *Chem. Rev.* **1993**, *93* (4), 1371−1448.
(98) Parks, D. J.; Blackwell, J. M.; Piers, W. E. *J. Org. Chem.* **2000**, *65* (10), 3090−3098.
(99) Parks, D. J.; Piers, W. E. *J. Am. Chem. Soc.* **1996**, *118* (39), 9440−9441.
(100) Rendler, S.; Oestreich, M. *Angew. Chem., Int. Ed.* **2008**, *47* (32), 5997−6000.
(101) Mewald, M.; Oestreich, M. *Chem. - Eur. J.* **2012**, *18* (44), 14079−14084.
(102) Sakata, K.; Fujimoto, H. *J. Org. Chem.* **2013**, *78* (24), 12505−12512.
(103) Ison, E. A.; Trivedi, E. R.; Corbin, R. A.; Abu-Omar, M. M. *J. Am. Chem. Soc.* **2005**, *127* (44), 15374−15375.
(104) Du, G.; Fanwick, P. E.; Abu-Omar, M. M. *J. Am. Chem. Soc.* **2007**, *129* (16), 5180−5187.
(105) Gutsulyak, D. V.; Vyboishchikov, S. F.; Nikonov, G. I. *J. Am. Chem. Soc.* **2010**, *132* (17), 5950−5951.
(106) Metsänen, T. T.; Hrobárik, P.; Klare, H. F. T.; Kaupp, M.; Oestreich, M. *J. Am. Chem. Soc.* **2014**, *136* (19), 6912−6915.
(107) Park, S.; Brookhart, M. *Organometallics* **2010**, *29* (22), 6057−6064.
(108) Dioumaev, V. K.; Bullock, R. M. *Nature* **2000**, *424* (6948), 530−532.
(109) Lipke, M. C.; Tilley, T. D. *J. Am. Chem. Soc.* **2014**, *136* (46), 16387−16398.
(110) Liberman-Martin, A. L.; Bergman, R. G.; Tilley, T. D. *J. Am. Chem. Soc.* **2015**, *137* (16), 5328−5331.

DOI: 10.1021/jacs.6b02173
J. Am. Chem. Soc. 2016, 138, 4972−4983

(111) Armarego, W. L. F.; Chai, C. *Purification of Laboratory Chemicals*, 7th ed.; Butterworth-Heinemann: Amsterdam, London, 2012.
(112) Enholm, E. J.; Jia, Z. J. *J. Org. Chem.* **1997**, *62*, 9159−9164.
(113) Ranu, B. C.; Banerjee, S. *Eur. J. Org. Chem.* **2006**, *2006*, 3012−3015.
(114) Weigend, F. *Phys. Chem. Chem. Phys.* **2006**, *8*, 1057−1065.
(115) Neese, F.; Wennmohs, F.; Hansen, A.; Becker, U. *Chem. Phys.* **2009**, *356*, 98−109.
(116) Retrieved from http://www.chemcraftprog.com. 2015.

DOI: 10.1021/jacs.6b02173
J. Am. Chem. Soc. 2016, 138, 4972−4983